Topological phase transitions in $(Bi_{1-x}In_x)_2Se_3$ and $(Bi_{1-x}Sb_x)_2Se_3$

Jianpeng Liu[1] and David Vanderbilt[1]

[1]*Department of Physics and Astronomy, Rutgers University, Piscataway, NJ 08854-8019, USA*

(Dated: October 7, 2013)

We study the phase transition from a topological to a normal insulator with concentration x in $(Bi_{1-x}In_x)_2Se_3$ and $(Bi_{1-x}Sb_x)_2Se_3$ in the Bi_2Se_3 crystal structure. We carry out first-principles calculations on small supercells, using this information to build Wannierized effective Hamiltonians for a more realistic treatment of disorder. Despite the fact that the spin-orbit coupling (SOC) strength is similar in In and Sb, we find that the critical concentration x_c is much smaller in $(Bi_{1-x}In_x)_2Se_3$ than in $(Bi_{1-x}Sb_x)_2Se_3$. For example, the direct supercell calculations suggest that x_c is below 12.5% and above 87.5% for the two alloys respectively. More accurate results are obtained from realistic disordered calculations, where the topological properties of the disordered systems are understood from a statistical point of view. Based on these calculations, x_c is around 17% for $(Bi_{1-x}In_x)_2Se_3$, but as high as 78%-83% for $(Bi_{1-x}Sb_x)_2Se_3$. In $(Bi_{1-x}Sb_x)_2Se_3$, we find that the phase transition is dominated by the decrease of SOC, with a crossover or "critical plateau" observed from around 78% to 83%. On the other hand, for $(Bi_{1-x}In_x)_2Se_3$, the In $5s$ orbitals suppress the topological band inversion at low impurity concentration, therefore accelerating the phase transition. In $(Bi_{1-x}In_x)_2Se_3$ we also find a tendency of In atoms to segregate.

PACS numbers: 71.23.An, 73.20.At, 03.65.Vf, 64.75.Nx, 71.70.Ej

I. INTRODUCTION

Topological aspects of quantum systems has been an exciting area in condensed-matter physics since the discovery of the integer quantum Hall effect (IQHE)[1,2] and the first proposal of a 2D Chern insulator.[3] Both the IQHE and the 2D Chern insulators are characterized by a quantized Hall conductance and the presence of gapless edge modes that are topologically protected by a non-zero Chern number. In 2005, a topological classification was also found to apply to spinful systems with SOC and time-reversal symmetry, defining a topologically non-trivial 2D state known as a quantum spin Hall (QSH) insulator.[4,5] A QSH insulator also possesses gapless edge states that always cross at one of the time-reversal invariant momenta (TRIM) in the 1D edge Brillouin zone (BZ). In a 2D Chern insulator, the chiral gapless edge modes can be interpreted in terms of the charge accumulation at one end of a truncated 1D system during an adiabatic periodic evolution. The spin-polarized edge modes in a QSH insulator can be interpreted in a similar way, except that charges with opposite spin characters are pumped in opposite directions and accumulated on opposite ends.[6] This pumping process can be classified by a new topological index, known as the $\mathbb{Z}_2$ index, which guarantees the robustness of the edge modes of a QSH insulator to weak time-reversal invariant perturbations.

The definition of the $\mathbb{Z}_2$ index was later generalized from 2D to 3D crystals.[7,8] In 3D systems, there is one strong $\mathbb{Z}_2$ index, which is odd when the number of Dirac cones on the surface is odd; when it is even, the other three indices characterize the weak TIs, specifying how these gapless surface states are distributed among the TRIM in the 2D surface BZ.

A non-trivial bulk topological index is usually connected with a non-trivial "topological gap" resulting from band inversion. For systems with inversion symmetry, the topological index can be uniquely determined from the parities of the occupied states at the TRIM in the BZ.[9] Thus, to drive an inversion-symmetric system from a normal insulator (NI) to a TI, a strong SOC is usually needed to flip the valence-band maximum (VBM) and conduction-band minimum (CBM) with opposite parities at one of the TRIM. The band gap after the topological band inversion is conventionally assigned with a minus sign, to be distinguished from the ordinary band gap in the $\mathbb{Z}_2$-even case. The scenario sketched above is exactly the mechanism in the Bi_2Se_3 class of TIs.[10–17] In Bi_2Se_3 with SOC turned off, the VBM and CBM states at Γ are built from Se $4p$ and Bi $6p$ orbitals in such a way as to have opposite parities. When SOC is turned on, the previous VBM is pushed up into the conduction bands, leading to an exchange of parities and a non-trivial $\mathbb{Z}_2$ index. As long as the inverted band gap remains and time-reversal symmetry is preserved, a single Dirac cone exhibiting a helical spin texture is guaranteed to exist at $\overline{\Gamma}$ in the surface BZ. For some useful recent reviews, see Refs. 18–20.

Up to now, however, only a few pioneering works[21–23] have focused on the topological phase transition from the TI to the NI state driven by non-magnetic substitution, and while the general picture of such a transition seems obvious, details remain unclear. In the simplest picture, one would expect the band gap of a TI to decrease linearly as a lighter element with weaker SOC is substituted, and the phase transition would occur when the bulk gap is closed. However, on a closer look, many questions arise. For example, the bandstructures of known TIs are mostly dominated by p orbitals, but what happens if the substituted element includes different valence orbitals such as s or d orbitals? More fundamentally, translational symmetry is lost for a randomly substituted system. In this case, how should one determine the topological properties of a system in which wavevector $\mathbf{k}$ is no longer a good quantum number, and what signature indicates the presence of a TI state? These questions focus on two aspects that are not taken into account in the simplest linear band-closure picture: the effects of impurities with different orbital character, and the effects of disorder.

These issues arise, in particular, for the substitution of In

into Bi_2Se_3, one of the best-known TI systems. Recently, several experimental groups have reported a surprisingly low critical concentration x_c of about 5% in $(Bi_{1-x}In_x)_2Se_3$, much lower than would be expected from a linear band-closure picture, thus challenging the usual understanding of the phase-transition behavior of TIs by non-magnetic doping.[24,25] These experiments motivated our theoretical studies of the $(Bi_{1-x}In_x)_2Se_3$ system. Moreover, to separate the effects of In $5s$ orbitals from a simple weakening of the effective SOC, we also study $(Bi_{1-x}Sb_x)_2Se_3$. Here Sb has the same orbital character as Bi, lying directly above it in the Periodic Table, but shares the weaker intrinsic SOC strength of In because their atomic numbers are very close in magnitude.

We first study the solid-solution systems by constructing small supercells with different impurity configurations. For each supercell configuration, the strong $\mathbb{Z}_2$ index and surface states are computed using Wannier-interpolation techniques,[26] which also allow us to test the effect of artificially removing the In $5s$ orbitals from the calculation. Next, we study the the effects of disorder more realistically by constructing a large supercell of pure Bi_2Se_3 acting as reference system, making random substitutions of In or Sb on the Bi sites, and calculating the disorder-averaged spectral functions.[27,28] We further propose an approach in which we compute "$\mathbb{Z}_2$-index statistics" in order to determine the topological properties of disordered systems from a statistical point of view.

Based on our results, the $(Bi_{1-x}Sb_x)_2Se_3$ system is well described by the linear band-closure picture with a high critical concentration x_c, because the orbital character of the host and dopant are the same and the disorder effect is thus rather weak. We also observe a "critical plateau" in the Sb-substituted system, where the critical Dirac semimetal phase remains robust from about $x \approx 78\%$ to $x \approx 83\%$, although it is difficult to test whether this may be a finite-size effect due to the limited numerical accuracy in our calculations. In In-substituted Bi_2Se_3, on the other hand, the disorder effects are quite strong, and the presence of In $5s$ orbitals rapidly drives the system into the NI state even at very low impurity concentrations. A tendency of segregation of In atoms has been observed for $(Bi_{1-x}In_x)_2Se_3$, and may play an important role.

The paper is organized as follows. In Sec. II the lattice structures, notations and the details of first-principles calculations are introduced. In Sec. III we present the main results of this paper. First we summarize the results from the direct first-principles superlattice calculations, and determine the critical points and the influence of In $5s$ orbitals by computing the bulk $\mathbb{Z}_2$ index and by calculating surface states. Then, the critical points of the two solid-solution systems are further determined by looking at the disordered spectral functions, and the topological behaviors are understood from a statistical point of view. Finally we summarize in Sec. IV.

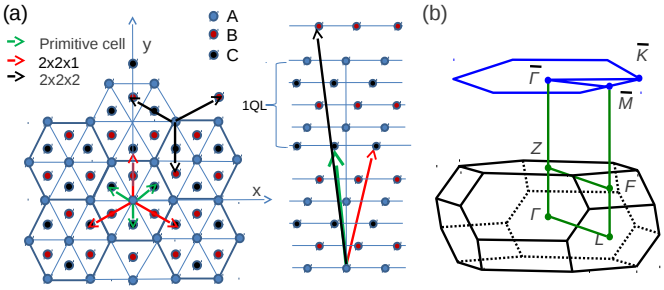

FIG. 1. (a) Lattice vectors of Bi_2Se_3 primitive cell, 2×2×1 supercell, and 2×2×2 supercell. (b) Corresponding bulk Brillouin zone and its surface projection.

II. PRELIMINARIES

A. Structures of bulk material and superlattices

As shown in Fig. 1, the crystal structure of Bi_2Se_3 is rhombohedral. The crystal has a layered structure along the z direction with five atoms per primitive cell. The five 2D monolayers made by repeating the primitive cell in the x and y directions form a quintuple layer (QL). In each QL, there are two equivalent Se atoms located at the top and bottom of the QL, two equivalent Bi atoms inside those, and another central Se atom. Seen from the top, each monolayer forms a 2D triangular lattice, and these triangular planes are stacked along the z direction in the order $A-B-C-A-B-C...$, where A, B and C represent the three different high-symmetry sites. Both Bi_2Se_3 and β-phase In_2Se_3 have a rhombohedral structure belonging to the $R\bar{3}$m space group, but their lattice parameters are slightly different. The in-plane hexagonal lattice parameter is $a = 4.138$ Å for Bi_2Se_3 but $a = 4.05$ Å for In_2Se_3, and the height of a QL is $c = 9.547$ Å for Bi_2Se_3 compared with $c = 9.803$ Å for In_2Se_3. The rhombohedral structure of Sb_2Se_3 does not exist in nature, so for this case we relaxed both the lattice parameters and atomic positions. After a complete relaxation, we obtained $a = 4.11$ Å and $c = 10.43$ Å for Sb_2Se_3.

To study the substitution problem from first-principles calculations, a 2×2×1 supercell based on the original Bi_2Se_3 crystal structure is built. The lattice vectors of the supercell are shown in Fig. 1. There are 20 atomic sites in such a supercell, where eight of them are Bi sites. Among all the possible configurations, we choose to investigate the supercells with one, two, four, six and seven Bi atoms substituted by impurities. The (unique) configuration with $x = 0.125$ is denoted as $C_{0.125}$. For two or six impurities ($x = 0.25$ and $x = 0.75$), there are two inequivalent configurations, with the two impurity (or remaining host) atoms residing in different monolayers or in the same monolayer, which we label as $C_{0.25}$ ($C_{0.75}$) and $C'_{0.25}$ ($C'_{0.75}$) respectively. For four impurities, $x = 0.5$, all impurities can be clustered in one monolayer, labeled as $C''_{0.5}$, or three in one monolayer and one in the other, denoted as $C'_{0.5}$, or the impurities can be equally divided between top and bottom monolayers with inversion symmetry, denoted as $C_{0.5}$. Note that primes indicate more strongly clustered con-

figurations.

B. First-principles methodology

The first-principles calculations are carried out with the QUANTUM ESPRESSO package,[29] with the PBE generalized gradient approximation (GGA) exchange-correlation functional[30,31] and well-tested fully relativistic ultrasoft[32] and norm-conserving pseudopotentials. The ultrasoft pseudopotentials are from QUANTUM ESPRESSO,[33] and the norm-conserving pseudopotentials are from the OPIUM package.[34,35] The ionic relaxations, ground-state energies, and densities of states presented in Sec. III are calculated with ultrasoft pseudopotentials, but we switched to norm-conserving pseudopotentials for those topics that required transformation to a Wannier representation (see below). The energy cutoff with ultrasoft pseudopotentials is 60 Ry for In-substituted Bi_2Se_3 supercells and 35 Ry for Sb-substituted supercells. The cutoff becomes larger for norm-conserving pseudopotentials, specifically 65 Ry for In substitution and 55 Ry for Sb substitution. The BZ is sampled on a $6\times6\times6$ Monkhorst-Pack[36] **k** mesh for the $2\times2\times1$ supercells, and $8\times8\times8$ for the primitive cell bulk materials. In our calculations, the lattice parameters of the Sb- and In-substituted supercells are fixed, taken as a linear interpolation of the Bi_2Se_3 and In_2Se_3 experimental lattice parameters according to the impurity concentration x, and the internal coordinates of the atoms are fully relaxed. We do not relax the lattice vectors because the coupling between two QLs is at least partially of van der Waals type, so that the standard GGA does not give a good estimate of the lattice constants, especially the one in the z direction.

To investigate the topological properties of these supercells, we calculate both the bulk $\mathbb{Z}_2$ indices and the surface states using the Wannier-interpolation technique. More specifically, we use the Wannier90 package to generate Wannier functions (WFs) from the outputs of standard first-principles calculations.[37] Wannier90 can optionally generate maximally localized WFs,[38,39] and in any case reports the Wannier charge centers, their spreads, and the real-space Hamiltonian matrix elements of an effective tight-binding (TB) model in the WF basis. This information is often very useful in studying the bonding mechanism of materials, as well as for calculating topological indices, computing surface and interface states, treating disorder, etc.

It should be noted that the TB models constructed from Wannier90 are realistic in the sense that the Wannier-interpolated bandstructures reproduce the first-principle bandstructures essentially exactly within a certain energy window. This "frozen window" is chosen to extend from 3 eV below the Fermi level to 3 eV above the Fermi level in our calculations. In addition to the frozen window, there is also an outer energy window outside which the Bloch eigenstates will not be included in generating the WFs. The outer window varies in our calculations depending on the system, but typically covers a total range of 17-22 eV and includes all the valence p bands as well as In valence s bands when present. For example, for Bi_2Se_3we construct 30 spinor WFs per primitive cell, and two additional WFs constructed from In valence s orbitals would be added for each substituted In atom.

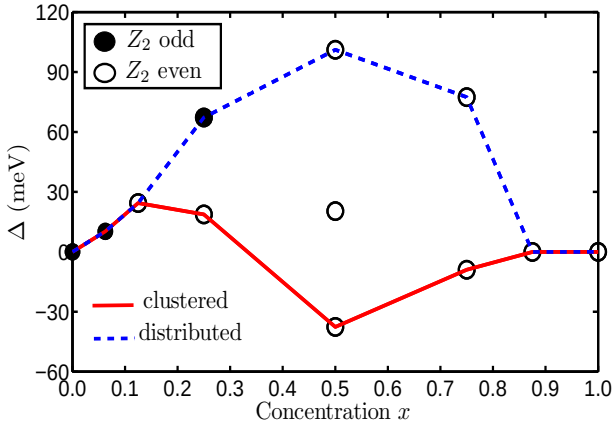

FIG. 2. Ground-state energies vs. impurity concentration x for $(Bi_{1-x}In_x)_2Se_3$ supercells. Here $\Delta = E_g(x) - (1-x)E_1 + xE_2$, where $E_g(x)$, E_1 and E_2 are the ground-state energies per 5-atom cell for the alloy supercell, host material, and dopant material, respectively. Filled and open circles denote $\mathbb{Z}_2$-odd and even states respectively. Solid (red) and dashed (dark blue) lines follow the most and least In-clustered configurations respectively.

III. RESULTS AND DISCUSSIONS

A. Ground-state energies and band gaps

We begin by discussing our results for In-substituted supercells representing $(Bi_{1-x}In_x)_2Se_3$. The ground-state energies for supercells with different In impurity configurations are shown in Fig. 2. Open and closed circles represent topologically normal and $\mathbb{Z}_2$-odd cases respectively (see Sec. III D). For concentrations $0.25 \le x \le 0.75$ there are two or more inequivalent configurations of the $2\times2\times1$ supercell having the same concentration x. Among these, the configurations with lowest total energy are traced by the solid red line, and are found to consist of "clustered" configurations in which the In impurities tend to be first neighbors. Conversely, those with the highest total energies, indicated by the dark blue dashed line, are those with the In atoms distributed most evenly throughout the supercell. For example, at $x=0.5$, the ground-state energy of the clustered configuration ($C''_{0.5}$) is lower than that of the distributed one ($C_{0.5}$) by 140 meV per primitive unit cell, and at $x=0.25$ the energy of $C'_{0.25}$ is lower than that of $C_{0.25}$ by 50 meV per primitive unit cell. Thus we clearly find a strong tendency of the In atoms to segregate and cluster together. We also find that the $\mathbb{Z}_2$ index changes sign at a critical concentration x_c lying somewhere between 6.25% and 12.5%. (One may notice from Fig. 2 that the distributed configuration $C_{0.25}$ at $x=0.25$ is $\mathbb{Z}_2$-odd, but since its energy is so much higher, the significance of this is questionable.)

Turning now to the case of Sb substitution, we find a quite different behavior. The corresponding total-energy results for the $2\times2\times1$ $(Bi_{1-x}Sb_x)_2Se_3$ supercells are presented in

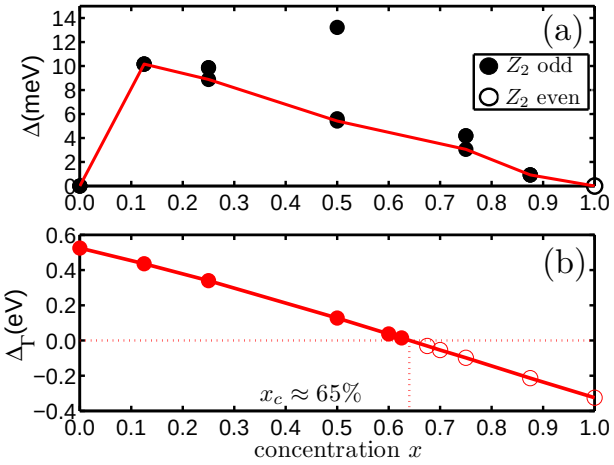

FIG. 3. (a) Ground-state energies vs. impurity concentration x for $(Bi_{1-x}Sb_x)_2Se_3$ supercells, following the same conventions as in Fig. 2. (b) Band gap at the center of the Brillouin zone vs. impurity concentration x computed within the virtual crystal approximation. Positive and negative values of band gap denote the topological and normal phases respectively.

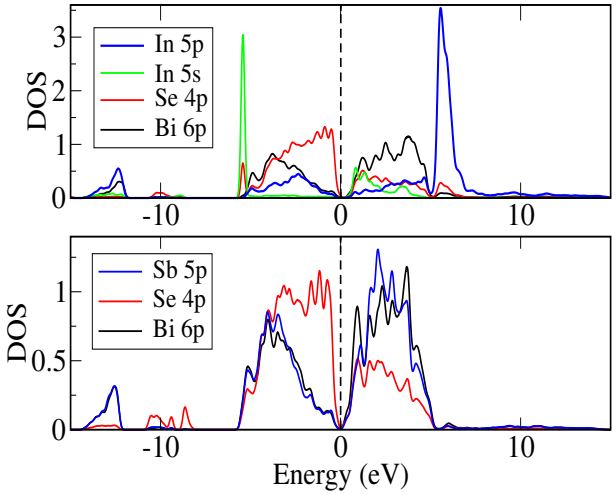

FIG. 4. (a) Local DOS of $(Bi_{1-x}In_x)_2Se_3$ at $x = 12.5\%$ for the s and p orbitals on the substituted In atom and the p orbitals on first-neighbor Bi and Se atoms. (b) Local DOS of $(Bi_{1-x}Sb_x)_2Se_3$ at $x = 12.5\%$ for the p orbitals on the substituted Sb atom and the p orbitals on first-neighbor Bi and Se atoms.

Fig. 3(a). Here we find that the energies of different configurations at the same x differ by no more than 10 meV per primitive unit cell, which is roughly ten times smaller than in $(Bi_{1-x}In_x)_2Se_3$ (note the difference in the vertical scales here compared to Fig. 2). This signifies that the disorder effect is very weak in this system. It is also evident from Fig. 3(a) that the system remains in the TI phase even up to $x = 87.5\%$, in sharp contrast to the behavior in $(Bi_{1-x}In_x)_2Se_3$.

Because we find the disorder effect to be so weak in Sb_2Se_3, we have also analyzed its behavior using the virtual crystal approximation (VCA), in which each Bi or Sb is replaced by an identical average atom whose properties are a weighted mean of the two constituents. We implement the VCA in a Wannier basis by constructing separate 30-band models for Bi_2Se_3 and Sb_2Se_3, including all the valence cation and anion p orbitals. The Hamiltonian matrix elements $H^{\rm VCA}_{mn}$ of the "virtual crystal" are taken as the linear interpolation in x of the two bulk materials, $H^{\rm VCA}_{mn} = (1-x)H^{\rm Bi}_{mn} + xH^{\rm Sb}_{mn}$, where $H^{\rm Bi}_{mn}$ and $H^{\rm Sb}_{mn}$ denote the matrix elements of the TB models of Bi_2Se_3 and Sb_2Se_3. We note in passing that one has to be cautious when generating the WFs for the VCA procedure, since it is important for the Wannier basis functions to be as similar as possible before the averaging takes place. Only in this way will the addition and subtraction between two different Hamiltonians be well defined. Because the maximal localization procedure might generate different WFs for different systems as it seeks to minimize the "spread functional,"[38] we construct the WFs for the VCA treatment simply by projecting the Bloch states onto the same set of atomic-like trial orbitals without any further iterative localization procedure.

Within this VCA approach, it is straightforward to compute the band gaps and topological indices, since only a primitive bulk cell is needed. Fig. 3(b) shows how Δ_Γ, the band gap at the Brillouin zone center, evolves with x for the $(Bi_{1-x}Sb_x)_2Se_3$ virtual crystal. It is evident that the gap closes at $x_c \simeq 65\%$, where the system undergoes a transition to the normal-insulator state (here indicated by a negative gap value).

B. Orbital character

To get some physical insight about the distinct behaviors in the two substituted systems, we turn to study the orbital character at a low composition of $x = 12.5\%$. The local density of states (DOS) of the substituted In and Sb atoms and their neighboring Bi and Se atoms are plotted in Fig. 4. For low-composition In-substituted systems, the In $5s$ orbitals and nearest-neighbor Se $4p$ orbitals form bonding and antibonding states, with the former leading to a flat band deep in the valence bands corresponding to the In $5s$ peak around -6 eV in Fig. 4(a). The hybridized s-p anti-bonding states further interact with the Bi $6p$ orbitals, bringing some In $5s$ character into the conduction bands. The In $5p$ orbitals are mainly responsible for the sharp peak about 7 eV above the Fermi level in Fig. 4(a), but also mix with Bi and Se p orbitals on the nearby atoms to contribute to the lower conduction-band states. The hopping between In $5p$ and neighboring Se $4p$ states, on the other hand, contributes mainly to the valence band, but also to the lower conduction bands.

If one only focuses on the low-energy physics, say within 5 eV of the Fermi level, one would notice that the In $5p$ states are homogeneously distributed among the valence and conduction bands. On the other hand, the s orbitals are more concentrated at the bottom of the valence and conduction bands. This implies that the effects of In $5s$ and $5p$ orbitals in the supercell electronic structure are distinct. The non-homogeneously distributed In $5s$ states may be crucial in determining the topological properties of the supercell. From the DOS at the Γ point (not shown here), we also observe that

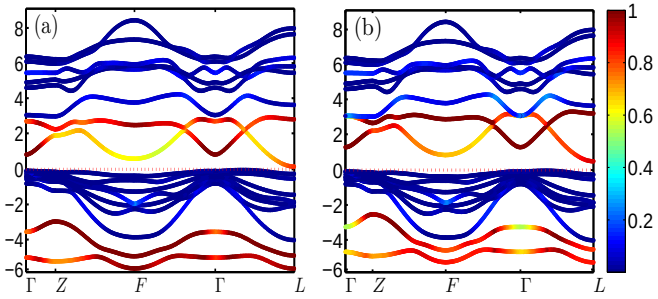

FIG. 5. (a) Wannier-interpolated bandstructure of In_2Se_3, with color code indicating In $5s$ character. (b) Same but with In $5s$ levels shifted upward by 0.79 eV.

the VBM is mostly composed of Se $4p$ states, while the CBM is dominated by Bi $6p$ states. This implies that the nontrivial topological band inversion has already been removed at 12.5% of In substitution.

For the Sb substitution at $x = 12.5\%$, however, the local DOS shown in Fig. 4(b) indicates that that Sb $5p$ orbitals are more or less homogeneously distributed among the valence and conduction bands as they hybridize with the Bi and Se p states. In fact, the Sb 5p and Bi 6p local DOS profiles are strikingly similar. While not displayed, we also explore the DOS of $(Bi_{1-x}Sb_x)_2Se_3$ at other compositions, and observe that the hybridization between Bi, Se and Sb p states remains homogeneous over the entire composition range. A homogeneous hybridization of Bi, Se and Sb p states tends to confirm the appropriateness of the use of VCA with artificial orbitals to construct an effective description of the electronic structure of the substituted system. Within the VCA, the strength of the effective SOC would be expected to decrease linearly as x is increased, suggesting that the topological phase transition in the Sb-substituted system should belong to the linear band-closure regime.

To study In-substituted Bi_2Se_3 at a lower concentration, a $2\times2\times2$ supercell has been constructed, in which one out of 16 Bi atoms is substituted by In. The supercell lattice vectors are shown in Fig. 1. The energy cutoff is taken to be the same as for the $2\times2\times1$ supercell calculations. A $3\times3\times3$ Monkhorst-Pack $\mathbf{k}$ mesh is used for ionic relaxation and calculation of the ground-state energy, while it is increased to $4\times4\times4$ for the non-self-consistent calculation used to interface with Wannier90. The ground-state energy is indicated by the filled circle at $x = 6.25\%$ in Fig. 2, and is confirmed to be in the $\mathbb{Z}_2$-odd phase from the $\mathbb{Z}_2$ index and surface-state calculations.

C. Shift of In 5*s* levels

Among the In-substituted configurations, our calculations find that $C_{0.5}$ and $C_{0.75}$ are metallic, in contrast with experimental observations showing the gap opening with increasing x beyond the transition to the normal phase.[24,25] The reason for the gap closure becomes clear from an inspection of our calculated bandstructure of bulk In_2Se_3, shown in Fig. 5(a), which was computed using the Wannier interpolation capabilities of the Wannier90 package[37] based on a 34-band TB model including the 30 valence p orbitals and four In $5s$ orbitals. The color coding in Fig. 5(a) shows the degree of In $5s$ character. We find that there is almost a gap closure, $E_g \simeq 0.15$ eV, much smaller than the experimental value of 1.34 eV.[40] Our small gap clearly results from a low-lying conduction band at L that is dominantly of In $5s$ character. For the $C_{0.5}$ and $C_{0.75}$ cases, these states get folded and mixed with other conduction-band states in such a way as to cause the metallic behavior observed in our supercell calculations.

We have good reason to believe, however, that the energy position of these In $5s$ is incorrectly predicted by standard density functional theory (DFT).[41,42] It is well known that DFT tends to underestimate gaps, especially when the character of the VBM (here p states at Γ) and the CBM (here In $5s$ states at L) are different. More specifically, however, quasiparticle calculations on InAs have shown that the In $5s$ energy levels are too low relative to the many-body GW calculation.[43] In particular, the CBM at Γ, having In $5s$ character, was found there to be too low by about 0.79 eV within DFT. We have checked that our In $5s$ energy positions do not depend sensitively on the use of the local-density approximation (LDA)[44] *vs.* GGA, the choice of pseudopotentials, or the use of different code packages.[45,46] Therefore, we conclude that more advanced approaches such as hybrid functionals or direct many-body methods are needed to fix this problem.

Unfortunately, application of hybrid functionals to our supercell calculations would be computationally expensive. Here we have taken a simpler approach to adjust the In $5s$ energy levels. The Wannier interpolation procedure has already provided us with a first-principles effective TB model reproducing the DFT bandstructure. We simply shift the energies of all the In $5s$ orbitals within this effective model upward by 0.79 eV, the value taken from Refs. 43, and leave all other matrix elements unchanged. The resulting bandstructure for bulk In_2Se_3 is shown in Fig. 5(b). We find that the band gap opens up to 0.52 eV, while otherwise the general character of bandstructure is not significantly changed.

While 0.52 eV is still far from an experimentally correct estimate of the gap, we expect our modified Wannier Hamiltonian should be good enough for the purpose of computing topological properties of $(Bi_{1-x}In_x)_2Se_3$ solid solutions. Once we apply this shift, we find that that the supercells that were metallic before are now insulating, and moreover the states near the Fermi energy that determine the topological character do not have significant In $5s$ character. Therefore, the magnitude of the shift is not important for computing the topological properties, as long as it is large enough to prevent the In $5s$ levels from interfering. In any case, since the β phase of In_2Se_3 is not very stable at room temperature (it has to be stabilized by doping small amounts of Sb),[40] a direct comparison between the experimental and theoretical band gaps is not very meaningful. Therefore, we adopt the procedure here of applying the 0.79 eV shift of In $5s$ levels in all of our In-substituted supercell calculations. In particular, the $\mathbb{Z}_2$ indices (filled *vs.* open circles) shown in Fig. 2 have been computed using this shift, as will be discussed in detail next.

D. $\mathbb{Z}_2$ indices

The strong $\mathbb{Z}_2$ indices of all the In and Sb-substituted Bi_2Se_3 supercells have been calculated in order to locate the critical concentrations for the transition from topological to normal behavior in the two solid-solution systems. As discussed above, some of the supercells ($C_{0.25}$, $C_{0.5}$ and $C_{0.75}$) have inversion symmetry, in which case the strong $\mathbb{Z}_2$ index can be evaluated simply by counting the parities of the occupied bands at the TRIM in the BZ. Specifically, if one defines δ_i as the product of the parities of the occupied bands (counting just one band from each Kramers doublet) at the ith TRIM in the BZ, the strong $\mathbb{Z}_2$ index is just $\nu_0 = \prod_{i=1}^{8} \delta_i$, i.e., the product of δ_i at all the eight TRIM.[47]

In the general case, however, the strong $\mathbb{Z}_2$ index has to be determined by explicitly calculating the 2D $\mathbb{Z}_2$ indices of the top and bottom slices of half of the 3D BZ. There are six such 2D indices, namely $\nu_j \equiv \nu_{k_j=0}$ and $\nu'_j \equiv \nu_{k_j=\pi}$, corresponding to the indices of the slices at $k_j = 0$ and $k_j = \pi$, where $j = \{1, 2, 3\}$ labels the three wavevector directions in the BZ. However, only four of the six indices turn out to be independent variables. The indices ν_1, ν_2 and ν_3 are usually taken to define the three weak topological indices, while the product $\nu_0 = \nu_j \nu'_j$ of the two indices on any pair of parallel slices is known as the strong $\mathbb{Z}_2$ index ν_0. This means that if two parallel slices have different $\mathbb{Z}_2$ indices, as for example at $k_3 = 0$ and $k_3 = \pi$, then ν_0 is odd and the system is a strong TI; otherwise it is a weak TI if any indices are odd, or normal if not.

In the absence of inversion symmetry, the 2D $\mathbb{Z}_2$ index is defined by the change of 1D "time-reversal polarization," say in the k_1 direction, as the other wavevector k_2 evolves from 0 to π. The time-reversal polarization can be explicitly visualized by tracing the 1D hybrid Wannier charge centers (WCCs)[38] in the k_1 direction as a function of k_2. The $\mathbb{Z}_2$ index is odd if the hybrid WCCs of the Kramers doublets switch partners during the evolution, and even otherwise.[6]

We implement these ideas in practice using the approach of Soluyanov and Vanderbilt,[48] in which the 2D $\mathbb{Z}_2$ index is obtained by counting the number of jumps of the "biggest gap" among the 1D hybrid WCCs during the evolution. The approach for computing the $\mathbb{Z}_2$ indices described above has been implemented in the Wannier basis using the matrix elements of the effective TB model and the WCCs generated from Wannier90.[37]

The results are shown in Figs. 2 and 3(a) by using filled circles to indicate cases in which the strong Z2 index is odd, while an open circle means it is even. In fact, none of the $\mathbb{Z}_2$-even configurations are found to be weak TIs, so open circles denote topologically normal insulators. If one follows the solid (red) lines in Fig. 2 and Fig. 3(a), which track the configurations with lowest energies, it is clear that for $(Bi_{1-x}In_x)_2Se_3$ the system becomes topologically trivial for $x > 6.25\%$. For $(Bi_{1-x}Sb_x)_2Se_3$, however, the TI phase is preserved up to 87.5%.

It should be emphasized again that a 0.79 eV shift has been added on the on-site In $5s$ energy levels in the effective TB models for the supercells of $(Bi_{1-x}In_x)_2Se_3$. However, except for $C_{0.5}$ and $C_{0.75}$, which are metallic without the shift, the $\mathbb{Z}_2$ indices of all the other configurations are unchanged by the application of this shift.

TABLE I. Bulk band gaps at Γ for $x = 12.5\%$ in $(Bi_{1-x}In_x)_2Se_3$. "Shifted" In $5s$ levels were raised by 0.79 eV (see text).

	without SOC (eV)	with SOC (eV)
In $5s$ levels unshifted	0.72	0.11
In $5s$ levels shifted	0.68	0.07
In $5s$ levels removed	0.42	−0.26

E. Effects of In $5s$ orbitals on bulk and surface states

To understand why the phase transition happens so rapidly in $(Bi_{1-x}In_x)_2Se_3$, we focus on the $x = 0.125$ supercell, and separately investigate the effects of In $5s$ orbitals and SOC on bulk bandstructure. As shown in Table I, without SOC the In $5s$ orbitals try to pull down the VBM, leading to a band gap as large as 0.7 eV at Γ, such that the SOC strength is not large enough to invert the CBM and VBM. If the In $5s$ orbitals are removed, however, the gap at Γ is only 0.42 eV without SOC, and when SOC is added back the band inversion reoccurs, with an inverted gap as large as 0.26 eV (denoted with a minus sign in Table I). We also notice that the shift of In $5s$ levels only changes the gap at Γ by 0.04 eV, and does not influence the topological behavior.

We continue to study the effects of In $5s$ orbitals on surface states by calculating the surface bandstructures both with and without In $5s$ orbitals. The surface bandstructures shown in Fig. 6 are calculated with the "slab method," where the first-principles TB models of slabs of In- and Sb-substituted Bi_2Se_3 with finite thickness stacked along the [111] direction have been constructed. This is done by extrapolating the matrix elements of the primitive unit cell TB model to multiple QLs along the [111] direction, then truncating at the two surfaces to enforce open boundary conditions. The 2D surface bandstructure is then obtained by directly diagonalizing the TB model of the slab.

It has to be noted that the surface states are not calculated self-consistently by doing such a truncation at the surface, because the Wannier functions close to the surface could be significantly deformed and the hopping parameters between orbitals close to the surface are expected to be different from those deep in the bulk. These effects are not properly included simply by truncating at the slab boundaries. However, we argue that even though these surface effects could be important in determining such details as the exact position of the Dirac point (if present) relative to the bulk CBM, they cannot change the topological character of the surface states, which is what we really care about here.

To understand the role of In $5s$ orbitals in the phase-transition process, the surface states are calculated both with and without the In $5s$ orbitals. The results for the configurations with lowest energy (the In-clustered configuration) are

TABLE II. Existence of topological surface states vs. impurity concentration x in $(Bi_{1-x}In_x)_2Se_3$ and $(Bi_{1-x}Sb_x)_2Se_3$ based on slab calculations in the Wannier representation.

	0%	6.25%	12.5%	25%	50%	75%	87.5%	100%
With In $5s$	✓	✓	×	×	×	×	×	×
Without In $5s$	✓	✓	✓	✓	×	×	×	×
Sb substitution	✓	-	✓	✓	✓	✓	✓	×

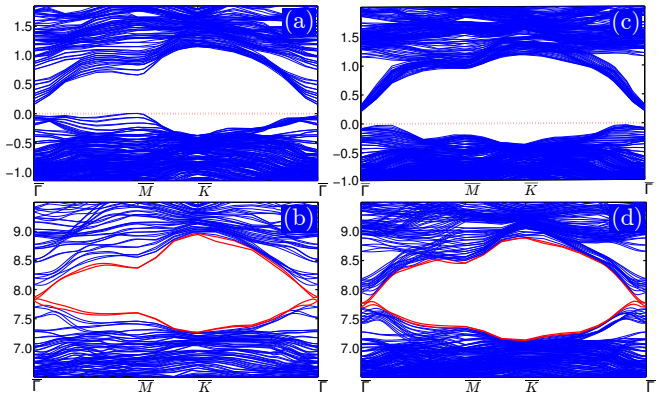

FIG. 6. Surface bandstructures for $(Bi_{1-x}In_x)_2Se_3$ slabs, plotted in the 2D surface Brillouin zone. (Surface states are shown in red.) (a) 8QL slab for $x = 0.125$. (b) 4QL slab for $x = 0.125$ but with In $5s$ orbitals removed. (c) 12QL slab for energetically favored configuration $C'_{0.25}$ at $x = 0.25$. (d) 8QL slab for $C'_{0.25}$ with In $5s$ orbitals removed. Note split Dirac cones arising at $\overline{\Gamma}$ in (b) and (d).

summarized in Table II, where '✓' indicates the existence of a Dirac cone around $\overline{\Gamma}$, and × denotes the absence of such a Dirac cone. The thicknesses of the slabs are chosen such that the interference between the states from two opposite surfaces is negligible.

As can be seen in Table II, the In $5s$ orbitals are directly responsible for removing the Dirac cones from the surface spectrum for the $C_{0.125}$ and $C'_{0.25}$ cases. This is shown explicitly in Fig. 6, where Dirac cones emerge at $\overline{\Gamma}$ only when the In $5s$ orbitals are removed. (Actually, a close inspection of the figure shows a split pair of Dirac cones contributed by opposite surfaces, where the splitting arises because of broken inversion symmetry due to the pattern of In substitution.) Scanning over the Sb-substituted Bi_2Se_3 supercells from $x = 0.125$ to 0.875, clear signatures of Dirac cones are observed for all of them (not shown here), consistent with the results of the bulk $\mathbb{Z}_2$-index calculations of Fig. 3(a).

Our surface-state calculations are consistent with the results of a recent scanning tunneling microscope (STM) study of the same system,[49] where a local suppression of density of states was observed in the topological surface states due to substitutional In atoms. Based on our supercell calculations, we conclude that this suppression of the topological surface states results from the In $5s$ orbitals, with an In concentration of $x = 0.125$ or $x = 0.25$ being sufficient to remove them entirely.

F. Disordered spectral functions

The previous superlattice calculations enabled us to capture some important physics of the phase-transition behavior, but it is still difficult to give a precise estimate of the critical concentrations because of the limited size of the supercells and the approach of studying one particular configuration at a time. Here we use the Wannier representation to construct ensembles representing the disordered systems in much larger supercells, in an attempt to study the effects of disorder in the phase-transition process more realistically and estimate the critical points more accurately.

Two issues arise when disorder is included. First, in a periodic lattice structure without any disorder, the eigenstates of are Bloch states which are perfectly coherent with infinite lifetime, and the wavevector $\mathbf{k}$ is a good quantum number. For such systems with nontrivial band topology, the easiest way to study the topological phase transition is to look at the band structure; a band-gap closure usually implies a phase transition from a topological to trivial insulator. In disordered systems, however, the "band-gap closure" is not so easy to recognize, because the Bloch functions are no longer the eigenstates of the system and a bandstructure is really not well-defined. Secondly, as we know, the $\mathbb{Z}_2$ index is computable for periodic lattices if the information of occupied Bloch states in the entire BZ is given. However, it is a difficult question how to define the $\mathbb{Z}_2$ index and determine the topological behavior of a realistic disordered system.

Our answer to the first issue is to look at the disorder-averaged spectral functions computed from a large supercell with different impurity configurations, but unfolded back to the BZ of the primitive unit cell. If the disorder is weak, one should see a sharp spectrum with narrow lifetime broadening, which means the quantum states would remain coherent over long distances. For strongly disordered systems, however, it is expected that the spectral functions should be strongly smeared out due to the strong randomness of the impurity scattering, and the quantum states would be localized around the impurities with a relatively short localization length.

We propose the "$\mathbb{Z}_2$-index statistics" to address the second problem. To be specific, several different impurity configurations are generated in our calculations at each impurity composition x, forming a representative ensemble of the disordered system, and we then compute the strong $\mathbb{Z}_2$ index for each configuration. If each configuration in the disorder ensemble is equally weighted, then when over half of the configurations are in the $\mathbb{Z}_2$-odd phase, we say that the disordered system can be statistically considered as a TI.

To calculate the disordered spectral functions, we use the Wannier effective-Hamiltonian approach as well as the technique of unfolding first-principle supercell bandstructures (spectral functions) as proposed by Ku and coworkers.[27,28] To be explicit, we first construct a TB model for a 4×4×3 supercell of pure Bi_2Se_3 whose matrix elements are extrapolated from the primitive-cell Bi_2Se_3 TB model. The 4×4×3 supercell of the bulk material acts as the reference system in which the Bi atoms are randomly substituted by the impurity atoms. For a 4×4×3 supercell, there are 240 atoms of which

96 are Bi-like, so the impurity composition x can be varied on the scale of one percent, enabling us to determine the critical point x_c with high precision.

The next procedure is to extract the Hamiltonian of a single impurity defined under the same WF basis. This is done by working in a small supercell (2×2×1 in our case) and subtracting the pure bulk-material Hamiltonian H^0 from the Hamiltonian H^s of a supercell containing one substituted impurity of type s. To set the notation, we label (5-atom) cells within the supercell by l, sites within the cell as τ, and orbitals within the cell as m. Then the impurity potential is constructed as

$$\Delta^s_{lm,l'm'}(\tau_s) = (H^s_{lm,l'm'}(0\tau_s) - H^0_{lm,l'm'}) \times P_{lm,l'm'}(\tau_s)\,. \quad (1)$$

This describes the change in the on-site energy if $(lm) = (l'm')$, or in the hopping if $(lm) \neq (l'm')$, induced by the presence of the impurity of type s on site τ_s in the central cell $l_s = 0$ of the small supercell. We define a "partition function"[28] $P_{lm,l'm'}(\tau_s)$ that is used to partition the contribution of the single impurity from the super-images in the neighboring supercells, such that the single impurity Hamiltonian is not influenced by the artificial periodicity of the supercell. In our calculations this partition function is chosen as

$$P(d) = \begin{cases} e^{-(d/r_0)^8} & \text{if } d \le d_{\rm c} \\ 0 & \text{otherwise} \end{cases} \quad (2)$$

where $d = d_{lm,l'm'}(\tau_s) \equiv |\mathbf{r}_{lm} - \mathbf{r}_{0\tau_s}| + |\mathbf{r}_{l'm'} - \mathbf{r}_{0\tau_s}|$ is chosen as a measure of the "distance" from the hopping matrix element $(lm, l'm')$ to the impurity site located at $\mathbf{r}_{0\tau_s}$.[28] Here we choose $d_{\rm c} = 8.69$ Å and $r_0 = 7.86$ Å. (We find that if $d_{\rm c} > 8.5$ Å and r_0 is chosen slightly smaller than or equal to $d_{\rm c}$, the impurity Hamiltonian becomes insensitive to small variations of $d_{\rm c}$ and r_0.) Our partition scheme has been tested to be able to reproduce the first-principles 2×2×1 supercell bandstructures at $x = 0.125$ and 0.25.

We extract this impurity potential once and for all for an In atom substituting for the top Bi atom in the quintuple-layer ($s = 1$) and again when it substitutes for the bottom Bi atom ($s = 2$). Then for a particular impurity configuration $\mathcal{R} = \{l_1 s_1, l_2 s_2, \ldots\}$ of the $4 \times 4 \times 3$ supercell, where $l_j s_j$ specifies the subcell and type of impurity and j runs over the impurities in the supercell, the effective Hamiltonian is taken as a linear superposition of the reference-system Hamiltonian H^0 and the single-impurity Hamiltonians residing on the specified sites in the large supercell, i.e.,

$$H^{\mathcal{R}}_{lm,l'm'} = H^0_{lm,l'm'} + \sum_j \Delta^{s_j}_{(l-l_j)m,(l'-l_j)m'}(\tau_j)\,. \quad (3)$$

The linear superposition of the matrix elements of different TB Hamiltonians is well-defined only when these Hamiltonians are treated under the same WF basis. In other words, each of the orbitals from the large supercell with impurities should map appropriately to the corresponding orbitals of the unperturbed reference system. For this reason, we skip the maximal localization procedure when generating the WFs, and instead simply use the projection method to generate a basis that remains in close correspondence to the atomic-like orbitals. Once the effective Hamiltonians has been obtained for an ensemble of impurity configurations representing a given concentration x, we calculate the spectral function for each, and unfold it from the highly compressed supercell BZ into the primitive-cell BZ.[27] Finally, the ensemble average of the unfolded spectral functions can then be taken to reflect the effects of disorder on the original bulk electronic states.

To be specific, let $A_N(\omega, \mathbf{K})$ be the spectral function at energy ω associated with band N in the supercell, with $\mathbf{K}$ specifying the wavevector in the small supercell BZ, given by the imaginary part of the retarded Green's function operator G via $A = -\pi^{-1}\,\mathrm{Im}\,G = -\pi^{-1}\,\mathrm{Im}(\omega + i\eta - H)^{-1}$, where H is the supercell Hamiltonian and $\eta > 0$ is a small artificial smearing factor. Then, to unfold the supercell spectral function onto a complete set of primitive-cell Bloch states, one can expand the primitive-cell spectral function $A_n(\omega, \mathbf{k})$ in terms of the supercell spectral functions as

$$A_n(\omega, \mathbf{k}) = \sum_{N\mathbf{K}} |\langle \psi_{N\mathbf{K}} | \psi_{n\mathbf{k}} \rangle|^2 A_N(\omega, \mathbf{K})\,, \quad (4)$$

where $|\psi_{n\mathbf{k}}\rangle$ and $|\psi_{N\mathbf{K}}\rangle$ are the primitive-cell and supercell Bloch states respectively, and n and $\mathbf{k}$ represent the band index and wavevector of the primitive cell. One can solve for the coefficient $\langle \psi_{N\mathbf{K}} | \psi_{n\mathbf{k}} \rangle$ within the Wannier basis provided that the supercell Hamiltonian is defined under a set of WFs having a clear one-to-one mapping with the primitive-cell WFs by primitive-cell lattice translations, as can be realized by using simple projection for the Wannier construction.[50]

In our calculations, 16 configurations are generated for $(Bi_{1-x}In_x)_2Se_3$ at each impurity composition, whereas eight configurations are generated for each x of $(Bi_{1-x}Sb_x)_2Se_3$ due to the much weaker effect of disorder. For $(Bi_{1-x}Sb_x)_2Se_3$ the configurations are generated randomly, as different configurations seem to be equally favored energetically. For $(Bi_{1-x}In_x)_2Se_3$, however, the configurations are generated using the Metropolis Monte Carlo method according to a proper Boltzmann weight in order to reflect the tendency of In segregation. The Boltzmann weight is proportional to $e^{-(E_p N_p)/(k_B T_g)}$, where $E_p = [E(\mathrm{C}'_{0.25}) - E(\mathrm{C}_{0.25})]/2$ is defined as the "paring energy" of In atoms, N_p is the number of In pairs in a particular configuration, k_B is the Boltzmann constant, and $T_g = 850°\mathrm{C}$ is taken as the growth temperature of the In-substituted Bi_2Se_3 sample.

The disordered spectral functions of $(Bi_{1-x}Sb_x)_2Se_3$ are shown in Fig. 7, with an artificial Lorentzian broadening of 2 meV. At $x = 68\%$, the spectral gap is visible, but already very small, suggesting that the system is approaching the critical point. As x is increased to 78%, a sharp Dirac cone is observed, which remains robust from 78% to 83%. At $x = 88.5\%$, the band gap reopens, meaning that the system is in the NI phase, and this topologically trivial phase becomes more robust as x goes to 99% with a more visible gap. One may notice that the effect of disorder is weak during the phase-transition process, and the semi-metallic behavior at criticality is rather sharp.

The spectral functions of $(Bi_{1-x}Sb_x)_2Se_3$ at the Γ point (in

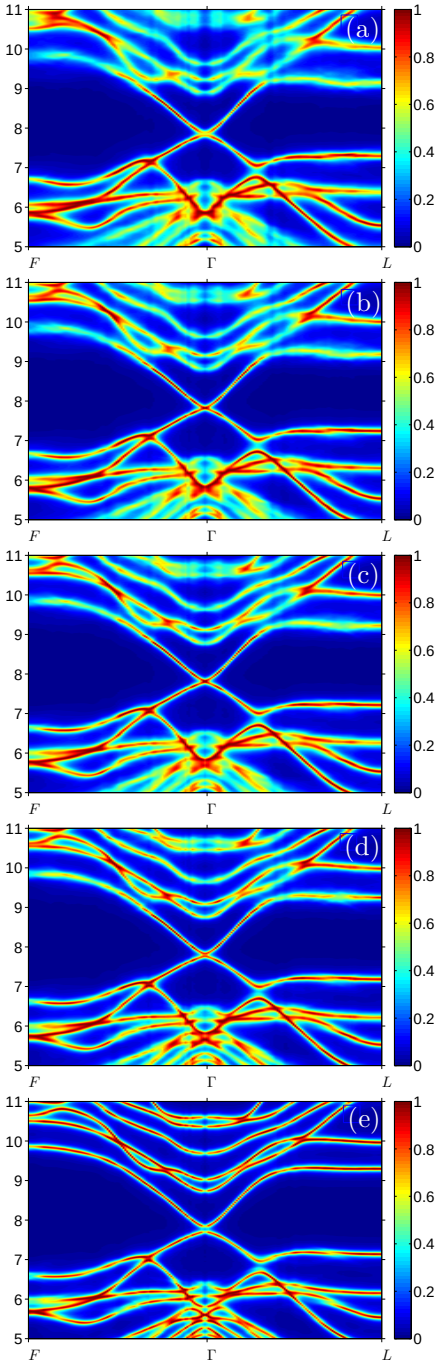

FIG. 7. Disordered spectral functions of $(Bi_{1-x}Sb_x)_2Se_3$ unfolded into the primitive-cell BZ. (a) $x = 68\%$. (b) $x = 78\%$. (c) $x = 83\%$. (d) $x = 88.5\%$. (e) $x = 99\%$.

the primitive-cell BZ) are plotted in Fig. 8. At $x = 68\%$ there are two peaks around the Fermi level, indicating that the CBM and VBM are still separated, and the critical point has not been reached yet. At $x = 78\%$ and 83%, the two peaks from the conduction and valence bands merge into one, suggesting the system becomes a semimetal. As x goes to 88.5%, the gap opens up again. From these results it appears that there is a kind of "critical plateau" for x between $\sim$78% and $\sim$83%.

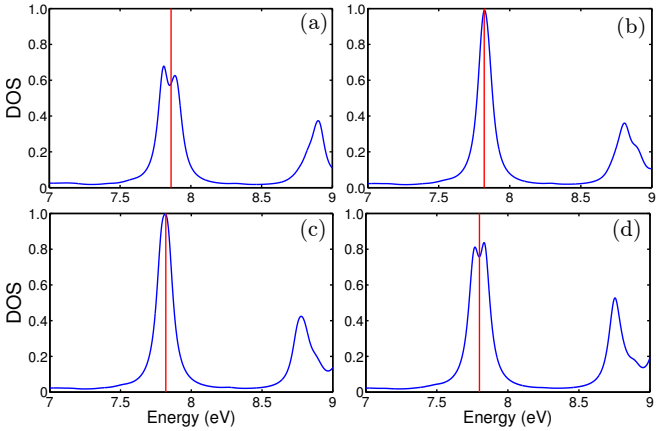

FIG. 8. Disordered spectral functions of $(Bi_{1-x}Sb_x)_2Se_3$ at the Γ point in the primitive-cell BZ for (a) $x = 68\%$, (b) $x = 78\%$, (c) $x = 83\%$, and (d) $x = 88.5\%$. Vertical (red) line indicates Fermi energy. Distinct VBM and CBM peaks are still visible in the topological phase in (a), merge in (b) and (c), and reappear in (d) as the gap reopens in the normal phase.

This critical behavior observed for $(Bi_{1-x}Sb_x)_2Se_3$ is at variance with the general expectation for the topological phase-transition behavior in the Bi_2Se_3 class of TIs, where the system becomes a critical Dirac semimetal at one point in the parameter space (here it is the impurity composition x) and then becomes insulating again immediately after the gap closure. This deserves discussion.

We cannot exclude the possibility that numeric uncertainties play a role here. In $(Bi_{1-x}Sb_x)_2Se_3$, the band gap varies quite slowly as a function of x, with a change of impurity composition of 5% corresponding to a band gap change of only $\sim$0.03 eV. Thus, the critical point could be hidden by disorder and artificial smearing, such that the system looks metallic even if a very small band gap has opened up. Moreover, finite-size effects may be important. In a disordered system we expect that the localization length evaluated in the middle of the mobility gap should grow as the mobility gap shrinks and the system approaches the critical metallic state. As one approaches the critical point at which this mobility gap vanishes, the localization length may exceed the size of the supercell and the states in neighboring supercells may overlap and behave like extended states.

However, it is also possible that a finite window of metallic phase is physically correct. Since the topologically nontrivial and trivial insulating configurations compete with similar weight near criticality, the system may remain in the metallic phase until one of the two insulating phases comes to dominate. Support for this picture can be drawn from Ref. 51, in which careful numerical simulations on a disordered lattice model showed a finite-width region of metallic phase as the system was driven from the TI to the NI phase with increasing disorder strength while other parameters were held fixed. In our case the disorder strength remains approximately constant, but the ratio of disorder strength to energy gap varies with x, so that a metallic plateau may still be expected. We leave these questions as avenues to pursue in future research.

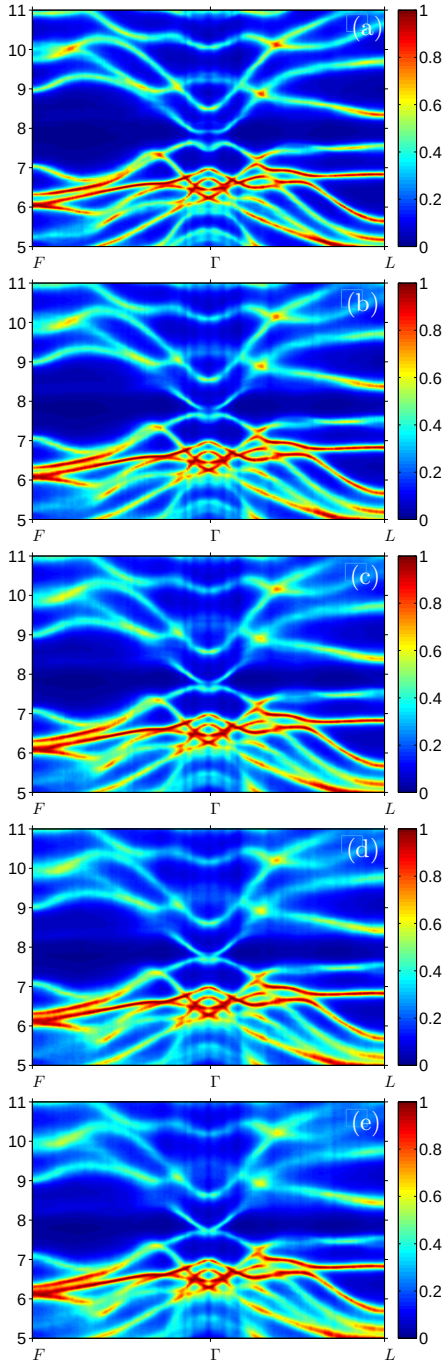

FIG. 9. Disordered spectral functions of $(Bi_{1-x}In_x)_2Se_3$ unfolded into the primitive-cell BZ. (a) $x = 8.3\%$. (b) $x = 12.5\%$. (c) $x = 14.6\%$. (d) $x = 16.7\%$. (e) $x = 18.8\%$.

The disorder-averaged spectral functions for $(Bi_{1-x}In_x)_2Se_3$ with the same artificial broadening are plotted in Fig. 9. At 8.3%, the band-inversion character is still obvious (note the tilde-like shape of the highest occupied bands around Γ) with the spectral gap unclosed, which implies the system may still stay in a TI phase. At 12.5% the spectral gap becomes hard to recognize. When it comes to 14.6%, 16.7% and 18.8%, the spectral gap is almost completely unrecognizable, which means the system is pretty close to the critical point. Moreover, in sharp contrast with the behavior of $(Bi_{1-x}Sb_x)_2Se_3$, the effect of disorder in $(Bi_{1-x}In_x)_2Se_3$ is very strong. It can be seen from Fig. 9 that the original energy bands are strongly smeared out. Different Bloch states are mixed together, as would be expected if localized eigenstates are formed centered on the substituted In atoms. It is difficult to identify the critical point simply by looking at the disordered spectral functions, because the Dirac semi-metallic behavior is not as obvious as in $(Bi_{1-x}Sb_x)_2Se_3$. Therefore, we calculate the $\mathbb{Z}_2$ index of each configuration from $x = 8\%$ to 18.8%. By inspecting the statistical behavior of the resulting $\mathbb{Z}_2$ indices, as described next, we conclude that the critical point of $(Bi_{1-x}In_x)_2Se_3$ is around 17%.

Our theoretical prediction of x_c for $(Bi_{1-x}In_x)_2Se_3$ is somewhat higher than the experimental values, estimated to be 3%-7% according to Brahlek *et al.*[24] and ∼6% according to Wu *et al.*[25] We attribute our overestimate of x_c to both the use of standard DFT methods and the absence of impurity-impurity correlation terms in Eq. (3). Regarding the former, we would expect to get an x_c more consistent with the experimental results if hybrid functionals or more advanced many-body first-principles methods were used in the calculations, which unfortunately becomes expensive for large supercells. Regarding the latter, we expect that the In clustering effects would be treated more accurately if we would go beyond a simple superposition of one-body impurity potentials and include many-body terms in the impurity cluster expansion when constructing the effective Hamiltonian. However, this too would carry a large computational cost due to the anisotropic nature of the two-body impurity-impurity interactions and the fact that higher-body terms may also be important.

G. $\mathbb{Z}_2$-index statistics

The $\mathbb{Z}_2$ indices of a 3D band insulator are well defined for a perfect periodic lattice with time-reversal symmetry. For disordered systems, however, the topological indices are much harder to calculate. A promising approach is the use of non-commutative algebra,[52–55] but to date this has generally been applied to simple models, and its applicability to realistic disordered materials has not been demonstrated.

Here we attempt to determine the topological indices of a disordered time-reversal invariant insulating system using a more straightforward approach: we calculate the strong $\mathbb{Z}_2$ index (with periodic boundary conditions on the supercell) for each impurity configuration in the statistical ensemble, thus determining the topological properties of the disordered system from a statistical point of view. As long as the configurations are sampled in such a way that each contributes equally to the statistical ensemble, then we define the system as $\mathbb{Z}_2$-odd (i.e., a strong TI) if over half of the configurations are $\mathbb{Z}_2$-odd, and normal otherwise. As mentioned in Subsec. III F, the impurity configurations of $(Bi_{1-x}In_x)_2Se_3$ are generated using the Metropolis Monte Carlo method based on a Boltzmann

TABLE III. $\mathbb{Z}_2$ statistics of $(Bi_{1-x}In_x)_2Se_3$. The entries in the first, second, and third rows indicate respectively the number of $\mathbb{Z}_2$-odd, $\mathbb{Z}_2$-even, and metallic configurations drawn from a 16-member ensemble.

	8.3%	12.5%	14.6%	16.7%	18.8%
$\mathbb{Z}_2$ odd	15	16	14	11	5
$\mathbb{Z}_2$ even	0	0	0	3	9
Metallic	1	0	2	2	2

weight defined by the In-clustering energy. As a result, the tendency of In segregation is reflected in the number of generated distributed vs. clustered configurations, rather than by manual assignment of weights. Thus we consider each configuration to be equally weighted, satisfying the criterion stated above.

The strong $\mathbb{Z}_2$ index statistics of several $(Bi_{1-x}In_x)_2Se_3$ configurations are shown in Table III. For x between 16.7 and 18.8%, the number of $\mathbb{Z}_2$-odd configurations drops from eleven to five, so we estimate x_c to be approximately 17%.

IV. SUMMARY AND OUTLOOK

To summarize, we have studied the topological phase transitions in $(Bi_{1-x}In_x)_2Se_3$ and $(Bi_{1-x}Sb_x)_2Se_3$ using two approaches, the direct application of first-principles calculations on small supercells, and a Wannier-based modeling approach that allows for a more realistic treatment of disorder in large supercells. Based on the former approach, the x_c of $(Bi_{1-x}In_x)_2Se_3$ is slightly less than 12.5%, while that of $(Bi_{1-x}Sb_x)_2Se_3$ is even above 87.5%. A VCA treatment of $(Bi_{1-x}Sb_x)_2Se_3$ predicts $x_c \sim 65\%$; this is not in perfect agreement with the prediction from the supercell calculations, but both of them are much higher than that of $(Bi_{1-x}In_x)_2Se_3$. From the results of realistic disordered calculations, we found that x_c is $\sim$17% for $(Bi_{1-x}In_x)_2Se_3$, while it is $\sim$78-83% for $(Bi_{1-x}Sb_x)_2Se_3$. The critical concentrations are determined from disorder-averaged spectral functions and $\mathbb{Z}_2$-index statistics. It is concluded that in $(Bi_{1-x}Sb_x)_2Se_3$, the band gap at Γ decreases almost linearly with increasing x, corresponding to the reduction in average SOC strength, with only a very weak disorder effect. For $(Bi_{1-x}In_x)_2Se_3$, on the other hand, the In $5s$ orbitals tend strongly to suppress the topological band inversion even at very low impurity concentrations, so that the phase transition is drastically accelerated as a function of increasing x.

In the case of $(Bi_{1-x}Sb_x)_2Se_3$, we observed a critical plateau from $x \sim 78\%$ to $x \sim 83\%$. As discussed in Subsec. III F, it is difficult to say whether this intermediate metallic phase is just an artifact of numerical limitations such as finite-size effects, or is a true feature of the physics. Further theoretical and experimental work is needed to clarify what happens in this critical region.

We also find a tendency of the In (but not Sb) atoms to segregate. This In clustering effect could help clarify some aspects of the topological phase transition in $(Bi_{1-x}In_x)_2Se_3$, as for example by suggesting a scenario in which the phase transition may happen locally, instead of homogeneously as in the usual linear gap-closure picture. One can imagine that as In atoms are implanted into bulk Bi_2Se_3, isolated In clusters would start to emerge, inside which the system is topologically trivial. As more and more Bi atoms are substituted by In, these isolated In "islands" become connected to each other, and the topological phase transition happens when the percolation threshold is reached.

Our results for $(Bi_{1-x}In_x)_2Se_3$ provide a physical explanation for the observed low transition concentration in several recent experiments on $(Bi_{1-x}In_x)_2Se_3$,[24,25] and the results on $(Bi_{1-x}Sb_x)_2Se_3$ may give predictions for future experimental works.

The techniques used in this paper provide a powerful methodology that may be used to carry out theoretical explorations of other types of disordered topological systems. For example, interesting physics is anticipated in a TI whose bandstructure is mostly contributed by p orbitals while substituting with impurities having d or f orbitals, or with non-vanishing magnetic moments. We thus hope that these methods will enable the search for new materials and systems with non-trivial topological properties in strongly disordered alloy systems.

ACKNOWLEDGMENTS

This work is supported by NSF Grant DMR-10-05838. We are grateful to M. Taherinejad and K. Garrity for useful discussions, I. Souza for important technical assistance with the codes, and W. Wu and his collaborators for sharing their unpublished experimental data.

[1] K. v. Klitzing, G. Dorda, and M. Pepper, Phys. Rev. Lett. **45**, 494 (Aug 1980).
[2] D. J. Thouless, M. Kohmoto, M. P. Nightingale, and M. den Nijs, Phys. Rev. Lett. **49**, 405 (Aug 1982).
[3] F. D. M. Haldane, Phys. Rev. Lett. **61**, 2015 (Oct 1988).
[4] C. L. Kane and E. J. Mele, Phys. Rev. Lett. **95**, 146802 (2005).
[5] C. L. Kane and E. J. Mele, Phys. Rev. Lett. **95**, 226801 (2005).
[6] L. Fu and C. L. Kane, Phys. Rev. B **74**, 195312 (2006).
[7] L. Fu, C. L. Kane, and E. J. Mele, Phys. Rev. Lett. **98**, 106803 (2007).
[8] J. E. Moore and L. Balents, Phys. Rev. B **75**, 121306 (2007).
[9] L. Fu and C. L. Kane, Phys. Rev. B **76**, 045302 (2007).
[10] H. Zhang, C.-X. Liu, X.-L. Qi, X. Dai, Z. Fang, and S.-C. Zhang, Nature Physics **5**, 438 (2009).
[11] C.-X. Liu, X.-L. Qi, H. J. Zhang, X. Dai, Z. Fang, and S.-C. Zhang, Phys. Rev. B **82**, 045122 (Jul 2010).

[12] D. Hsieh, Y. Xia, D. Qian, L. Wray, F. Meier, J. H. Dil, J. Osterwalder, L. Patthey, A. V. Fedorov, H. Lin, A. Bansil, D. Grauer, Y. S. Hor, R. J. Cava, and M. Z. Hasan, Phys. Rev. Lett. **103**, 146401 (Sep 2009).

[13] Y. Xia, D. Qian, D. Hsieh, L. Wray, A. Pal, H. Lin, A. Bansil, D. Grauer, Y. Hor, R. Cava, *et al.*, Nature Physics **5**, 398 (2009).

[14] D. Hsieh, Y. Xia, L. Wray, D. Qian, A. Pal, J. Dil, J. Osterwalder, F. Meier, G. Bihlmayer, C. Kane, *et al.*, Science **323**, 919 (2009).

[15] L. Wray, S. Xu, Y. Xia, D. Hsieh, A. Fedorov, Y. San Hor, R. Cava, A. Bansil, H. Lin, and M. Hasan, Nature Physics **7**, 32 (2010).

[16] D. Hsieh, Y. Xia, D. Qian, L. Wray, J. Dil, F. Meier, J. Osterwalder, L. Patthey, J. Checkelsky, N. Ong, *et al.*, Nature **460**, 1101 (2009).

[17] Y. L. Chen, J. G. Analytis, J.-H. Chu, Z. K. Liu, S.-K. Mo, X. L. Qi, H. J. Zhang, D. H. Lu, X. Dai, Z. Fang, S. C. Zhang, I. R. Fisher, Z. Hussain, and Z.-X. Shen, Science **325**, 178 (2009).

[18] M. Z. Hasan and C. L. Kane, Rev. Mod. Phys. **82**, 3045 (Nov 2010).

[19] X.-L. Qi and S.-C. Zhang, Rev. Mod. Phys. **83**, 1057 (Oct 2011).

[20] W. Feng and Y. Yao, Science China Physics, Mechanics and Astronomy **55**, 2199 (2012).

[21] T. Sato, K. Segawa, K. Kosaka, S. Souma, K. Nakayama, K. Eto, T. Minami, Y. Ando, and T. Takahashi, Nature Physics **7**, 840 (2011).

[22] S. Xu, Y. Xia, L. Wray, S. Jia, F. Meier, J. Osterwalder, B. Slomski, A. Bansil, H. Lin, R. Cava, *et al.*, Science **332**, 560 (2011).

[23] S. Chadov, J. Kiss, C. Felser, K. Chadova, D. Ködderitzsch, J. Minár, and H. Ebert, arXiv preprint arXiv:1207.3463(2012).

[24] M. Brahlek, N. Bansal, N. Koirala, S.-Y. Xu, M. Neupane, C. Liu, M. Z. Hasan, and S. Oh, Phys. Rev. Lett. **109**, 186403 (Oct 2012).

[25] L. Wu, R. V. Aguilar, M. Brahlek, A. V. Stier, Y. Lubashevsky, C. M. Morris, L. S. Bilbro, N. Bansal, S. Oh, and N. P. Armitage, arXiv preprint arXiv:1209.3290v2(2013).

[26] N. Marzari, A. A. Mostofi, J. R. Yates, I. Souza, and D. Vanderbilt, Rev. Mod. Phys. **84**, 1419 (Oct 2012).

[27] W. Ku, T. Berlijn, and C.-C. Lee, Phys. Rev. Lett. **104**, 216401 (May 2010).

[28] T. Berlijn, D. Volja, and W. Ku, Phys. Rev. Lett. **106**, 077005 (Feb 2011).

[29] P. Giannozzi, S. Baroni, N. Bonini, M. Calandra, R. Car, C. Cavazzoni, D. Ceresoli, G. L. Chiarotti, M. Cococcioni, I. Dabo, A. Dal Corso, S. de Gironcoli, S. Fabris, G. Fratesi, R. Gebauer, U. Gerstmann, C. Gougoussis, A. Kokalj, M. Lazzeri, L. Martin-Samos, N. Marzari, F. Mauri, R. Mazzarello, S. Paolini, A. Pasquarello, L. Paulatto, C. Sbraccia, S. Scandolo, G. Sclauzero, A. P. Seitsonen, A. Smogunov, P. Umari, and R. M. Wentzcovitch, Journal of Physics: Condensed Matter **21**, 395502 (19pp) (2009).

[30] J. P. Perdew, K. Burke, and M. Ernzerhof, Phys. Rev. Lett. **78**, 1396 (Feb 1997).

[31] J. P. Perdew, K. Burke, and M. Ernzerhof, Phys. Rev. Lett. **78**, 1396 (Feb 1997).

[32] D. Vanderbilt, Phys. Rev. B **41**, 7892 (1990).

[33] We used the pseudopotentials Bi.rel-pbe-dn-rrkjus.UPF, Se.rel-pbe-n-rrkjus.UPF, Sb.rel-pbe.US.UPF and In.rel-pbe-dn-rrkjus.UPF from `http://quantum-espresso.org`.

[34] `http://opium.sourceforge.net/`.

[35] N. J. Ramer and A. M. Rappe, Phys. Rev. B **59**, 12471 (May 1999).

[36] H. J. Monkhorst and J. D. Pack, Phys. Rev. B **13**, 5188 (Jun 1976).

[37] A. A. Mostofi, J. R. Yates, Y. S. Lee, I. Souza, D. Vanderbilt, and N. Marzari, Computer Phys. Comm. **178**, 685 (2008).

[38] N. Marzari and D. Vanderbilt, Phys. Rev. B **56**, 12847 (1997).

[39] I. Souza, N. Marzari, and D. Vanderbilt, Phys. Rev. B **65**, 035109 (2001).

[40] D. Eddike, A. Ramdani, G. Brun, J. Tedenac, and B. Liautard, Materials research bulletin **33**, 519 (1998).

[41] P. Hohenberg and W. Kohn, Phys. Rev. **136**, B864 (Nov 1964).

[42] W. Kohn and L. J. Sham, Phys. Rev. **140**, A1133 (Nov 1965).

[43] X. Zhu and S. G. Louie, Phys. Rev. B **43**, 14142 (Jun 1991), the CBM of InAs at Γ is dominated by In 5s orbitals.

[44] J. P. Perdew and A. Zunger, Phys. Rev. B **23**, 5048 (May 1981).

[45] `http://www.wien2k.at/`.

[46] G. Kresse and J. Furthmüller, Phys. Rev. B **54**, 11169 (1996).

[47] L. Fu and C. L. Kane, Phys. Rev. B **76**, 045302 (Jul 2007).

[48] A. A. Soluyanov and D. Vanderbilt, Phys. Rev. B **83**, 235401 (JUN 2 2011).

[49] Q. Shen, X. Wang, S.-W. Cheong, and W. Wu, unpublished.

[50] Expressed under Wannier basis, the summation over $\mathbf{K}$ in Eq. (4) becomes unnecessary, because there is a Kronecker-δ relationship between $\mathbf{k}$ and $\mathbf{K}$ in the expression for $\langle\psi_N(\mathbf{K})|\psi_n(\mathbf{k})\rangle$, thus removing the summation.

[51] B. Leung and E. Prodan, Phys. Rev. B **85**, 205136 (May 2012).

[52] J. Bellissard, A. van Elst, and H. Schulz-Baldes, Journal of Mathematical Physics **35**, 5373 (1994).

[53] E. Prodan, Journal of Physics A: Mathematical and Theoretical **44**, 113001 (2011).

[54] H. Schulz-Baldes and S. Teufel, Communications in Mathematical Physics **319**, 649 (2013).

[55] B. Leung and E. Prodan, Journal of Physics A: Mathematical and Theoretical **46**, 085205 (2013).